

Cite this: *Chem. Sci.*, 2012, **3**, 2307

www.rsc.org/chemicalscience

EDGE ARTICLE

Conformational effects in sugar ions: spectroscopic investigations in the gas phase and in solution†

Ram Sagar,^a Svemir Rudić,^{ab} David P. Gamblin,^a Eoin M. Scanlan,^a Timothy D. Vaden,^b Barbara Odell,^a Timothy D. W. Claridge,^a John P. Simons^{*b} and Benjamin G. Davis^{*a}

Received 18th March 2012, Accepted 25th April 2012

DOI: 10.1039/c2sc20341c

We present direct investigations of the conformational preferences of sugars with a positively charged substituent at their anomeric centre, C-1, which display in solution, a preference for an equatorial conformation—an apparent reversal of the normal anomeric effect. The investigations focus on the protonated monosaccharide, D-xylopyranosyl imidazolium in its α and β forms, first probed in a range of different solvents through NMR measurements and then in the gas phase, free of solvent or counterion interactions, through infrared multiphoton dissociation spectroscopy. The results, when compared and discussed in the light of density functional theory, *ab initio* and natural bond orbital calculations, expose the possible origins of the reversed conformational preference and provide a better understanding of the factors controlling conformational choice.

Introduction

In 1965 Lemieux and Morgan¹ reported the unexpected observation of an inverted, 1C_4 , pyranose ring conformation in an ionic sugar, per-acetylated α -D-glucopyranosyl pyridinium, which reversed the axial (and equatorial) orientations of the pyridinium (and acetate) groups. The conventional anomeric effect, which favours the axially oriented α anomer, no longer appeared to be dominant and it was described as a “reverse anomeric effect” (or RAE), see Fig. 1.¹ Similar conformational changes were later identified in a series of protonated *N*-glycosides.^{2–5}

Subsequent investigations explored its theoretical basis to distinguish between cause and effect, through semi-empirical and

ab initio calculations,^{6,7} but many others questioned its reality—and its definition.^{8–16} Perrin *et al.* for example,¹¹ discussed two different measures of the RAE, one based on the equilibrium between the normal (4C_1) and inverted (1C_4) conformers of the α anomer; the other on the equilibrium between the α and β anomers of the 4C_1 conformers, which forms the basis for the definition of the normal anomeric effect. Based on the second measure and comparing solution equilibria between the α and β anomers of a series of D-glucosylamines¹⁰ and subsequently, *N*-(glycopyranosyl) imidazole¹² and aniline¹³ derivatives, Perrin *et al.* found no evidence for a reversal of the normal anomeric effect.¹¹ Similar conclusions were reached using *N*-aryl *gluco*- and 5-thio-*gluco*-pyranosylamines;¹⁴ simplified 1,3-dioxolane ring systems bearing quaternary quinuclidinium substituents;¹² model furanosides;¹⁵ and molecules incorporating phosphonium rather than ammonium substituents.^{16,17}

Since all of these experimental investigations were conducted in solution, it was not possible to exclude environmental interactions with the solvent and the counterions, which might have clouded or even overwhelmed the normal anomeric effect; indeed, it was argued that Lemieux and Morgan's original observations may be entirely attributed to such environmental effects.⁹ On the other hand, an early *ab initio* (MP2/6-31G**/HF/6-31G*) calculation conducted for *isolated* 2-tetrahydropyranosyl ammonium by Cramer,⁷ predicted the axial (4C_1) anomer to be less stable, by 9.4 kJ mol⁻¹, than the corresponding (4C_1) equatorial anomer. On *this* measure, which is similar to the one preferred by Perrin¹¹ (though based on energy differences at 0 K rather than free energy differences at ~300 K) the reversal was described as “in seeming contravention of the normal anomeric effect”.⁷

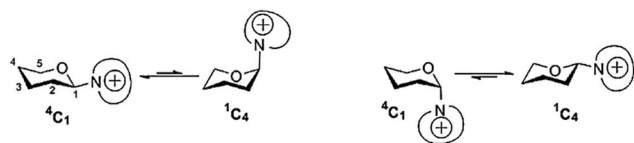


Fig. 1 Positively-charged anomeric substituents show a propensity for equatorial orientation, described as a “reverse anomeric effect”.

^aDepartment of Chemistry, University of Oxford, Chemistry Research Laboratory, Mansfield Road, Oxford OX1 3TA, UK. E-mail: ben.davis@chem.ox.ac.uk; Fax: +44 (0)1865 285002; Tel: +(0)1865 275652

^bDepartment of Chemistry, Physical and Theoretical Chemistry Laboratory, South Parks Road, Oxford OX1 3QZ, UK. E-mail: john.simons@chem.ox.ac.uk; Fax: +44 (0)1865 275410; Tel: +(0)1865 275400

† Electronic supplementary information (ESI) available: synthetic methods; NMR data; computed relative energies, vibrational frequencies and structural data. See DOI: 10.1039/c2sc20341c

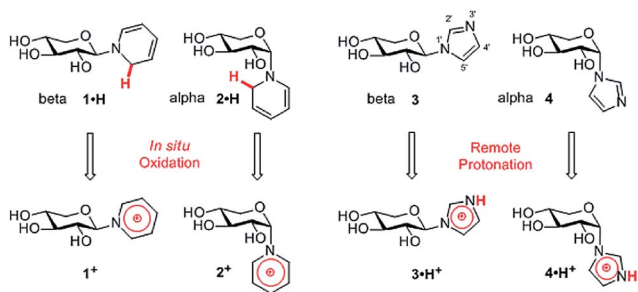


Fig. 2 Alternative strategies examined here to generate sugar cations in the gas phase with minimal steric or intramolecular perturbation. Either, *in situ* oxidation of neutral, oxidatively-sensitive, dihydropyridine precursors, **1·H** and **2·H**, to generate corresponding pyridiniums (**1⁺** and **2⁺**) through gas phase hydride loss-aromatization; or remote protonation of distal N-3' of imidazole of neutral *N*-glycosides **3** and **4** to create imidazoliums (**3·H⁺** and **4·H⁺**).

These matters have rested for most of the past decade. In the last year, however, new techniques have been devised which make it possible to probe the conformational preferences of isolated sugar ions in the gas phase, in the absence of solvents or counterions.¹⁸ Their application to a sugar displaying an apparent reversal of the normal anomeric effect should, in combination with theory, help to provide a better understanding of the factors controlling conformational choice, free from any external interactions. Following this aspiration, we present the first direct investigation of the conformational preferences of a conformationally labile, or 'spring-loaded'⁵ exemplar of the

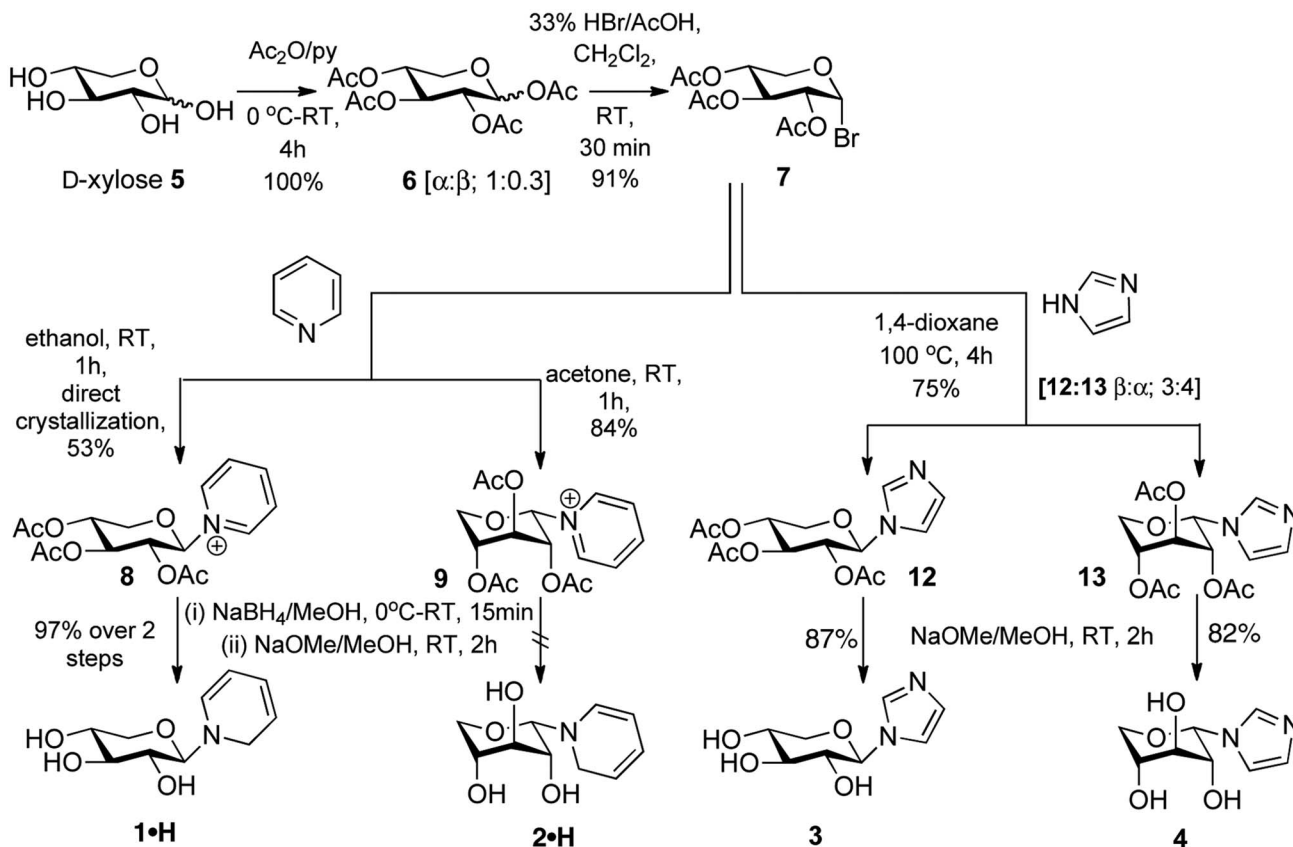
effect, the protonated monosaccharide, D-xylopyranosyl imidazolium in its α and β forms in the gas phase. The sugar ions are generated at a temperature of ~ 300 – 350 K, comparable to that in solution, and probed through IR laser spectroscopy. The results are then compared with those obtained in solution through NMR measurements and discussed in the light of density functional theory, *ab initio* and natural bond orbital calculations, to expose the intrinsic origins of the reversed conformational preference.

Results and discussion

Sugar ion precursors

Initially, two alternative strategies for generating cationic sugars in the gas phase were investigated: (a) *in situ* photo-oxidation of an *N*-glycosyl dihydropyridine, **1·H**, **2·H** to form the pyridinium ions **1⁺**, **2⁺** and (b) remote protonation of an *N*-glycosyl imidazole, **3**, **4** to form the imidazolium ions **3·H⁺**, **4·H⁺**, see Fig. 2.

To access the required dihydropyridines (DHPs) a two-step procedure was employed (Scheme 1) that would allow reduction of the pyridinium substituent in **8** or **9** to a DHP group, using a hydride source such as NaBH_4 followed by Zemplén methanalytic removal of the acetate protecting groups. This proceeded smoothly for β pyridinium **8** to yield the neutral β precursor **1·H** (see Electronic Supplementary Information†). Although the *in situ* photo-oxidation of **1·H** to yield pyridinium **1⁺** was successful, (see Fig. 5 below), the corresponding α anomer **2·H** proved highly sensitive. Despite the use of a range of



Scheme 1 Synthesis of neutral precursors **1·H**, **2·H**, **3**, **4**.

methods (alternative reductants and solid-supported variants), different procedures and even preparation under strict (glove box) inert atmosphere conditions, only decomposed or unreacted material was obtained from α pyridinium **9**, precluding a study of the pyridinium **2**⁺. An IR analysis of the unwanted by-products suggested the absence of OH-2 consistent with intramolecular cyclization of OH-2 onto the heterocyclic ring (see Supplementary Information†).

In contrast, deprotection of the *N*-imidazoles **12**, **13** (Scheme 1) proceeded smoothly and under Zemplén conditions directly yielded the neutral imidazoles **3** and **4**. These proved not only to be stable but readily handled under conditions used to study their conformations and importantly, those of their corresponding ions **3**·H⁺ and **4**·H⁺, both in the gas phase and in solution.

Conformations in solution: NMR spectroscopy

The NMR spectrum of **3** in D₂O (Fig. 3) revealed large coupling constants between H1 and H2 ($J_{1,2} = 9.2$ Hz) and between H2 and H3 ($J_{2,3} = 9.2$ Hz) indicating a diaxial orientation; the diaxial coupling constant between H5ax and H4 was also large ($J_{5ax,4} = 10.6$ Hz). This could only be understood if the pyranose ring adopted a ⁴C₁ conformation in aqueous solution (Table 1). When the imidazole moiety was protonated (through titration

with trifluoroacetic acid, TFA) to give **3**·H⁺, there was little change in its spectrum (Fig. 3a,b) apart from a de-shielding of the imidazole proton, H2', from δ 7.83 to 8.95 ppm which clearly indicated protonation of the imidazole ring. H2 was slightly shielded (from δ 3.73 to 3.62 ppm) but the typical diaxial coupling constants were unchanged. Characteristic nuclear Overhauser effects (NOEs) between H1–H5ax and H1–H3 provided further support for the continued population of *only* the ⁴C₁ conformer following protonation of the β ion (Fig. 3e).

In contrast, the NMR data for the neutral α anomer **4** were all consistent with a dynamic conformational equilibrium (Fig. 3c and Table 1). The ³*J* coupling constants, between H2–H3 and H3–H4 ($J_{2,3} = 5.6$ and $J_{3,4} = 5.1$ Hz), indicated averaged values lying between the two extremes³ of completely diaxial, ⁴C₁ conformer, $J_{2,3} = 9.3$ and $J_{3,4} = 9.5$ Hz, and completely diequatorial, ¹C₄ conformer, $J_{2,3} = 3.0$ and $J_{3,4} = 2.8$ Hz, (see Supplementary Information† Table S2). Variable temperature NMR measurements in CD₃OD (Supplementary Information† Figure S4) confirmed the dynamic interconversion. NOE experiments also revealed H1–H2 and H1–H5ax correlations indicating population of the ¹C₄ conformer (though they could not exclude population of the ⁴C₁ conformer as well, where an H1–H2 NOE would also be anticipated).‡ The coupling constant between H1 and H2 ($J_{1,2} = 3.0$ Hz) reflected the α glycoside structure.

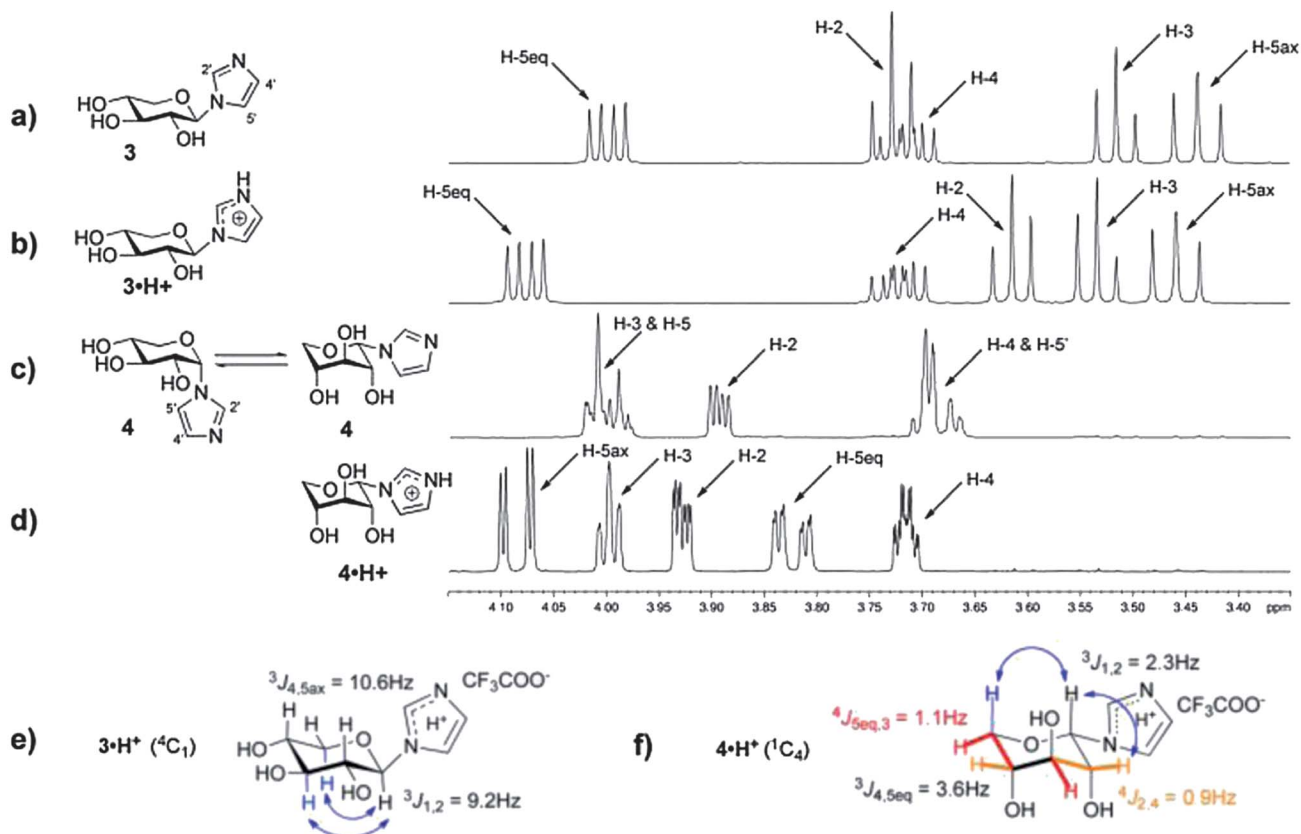


Fig. 3 Solution phase analysis. (a,b): Conversion of the neutral β -anomer **3** to ion **3**·H⁺ barely changes the ¹H NMR spectrum or the key coupling constants (Table 1) indicating maintenance of the ⁴C₁ conformation and an equatorial positively-charged substituent. (c,d): For the α -anomer, a broad set of signals and intermediate constants (Table 1) for coupling indicate a dynamic equilibrium between ⁴C₁ and ¹C₄ conformers in the neutral **4** but conversion to the ion **4**·H⁺ increases the ¹C₄ conformer (see Supplementary Information†). (e,f) Summary of indicative coupling values and NOEs for **3**·H⁺, **4**·H⁺: 3-bond coupling values shown in black; longer-range 4-bond ‘W-coupling’ values in red and orange; and key NOE enhancements in blue.

The NMR spectrum (Fig. 3d) of the protonated α anomer $4\cdot\text{H}^+$, was quite different. Protonation was confirmed by the deshielding of the imidazole proton H2', from δ 7.90 to 8.91 ppm (which did not change on continued addition of TFA). H2 centred at δ 3.93 showed couplings with H3 and H1 ($J_{2,3} = 4.9$ Hz, $J_{2,1} = 2.3$ Hz) along with very specific long range, 4-bond 'W-coupling' with H4 (${}^4J_{2,4} = 0.9$ Hz) typical of a ${}^1\text{C}_4$ conformation (Fig. 3f, Table S2†); H3 centred at δ 4.00 showed long range 'W-coupling' with H5eq (${}^4J_{3,5\text{eq}} = 1.1$ Hz); and assignment of ${}^1\text{C}_4$ as the major conformer was supported by NOE enhancements involving H1–H2 and H1–H5ax (Fig. 3f). Population of skew and half-chair conformers can be discounted since they were predicted by the DFT and *ab initio* calculations to lie at least 25 kJ mol⁻¹ higher in energy (in the gas phase). If the chair conformers are also the only ones populated in solution, the observed and limiting $J_{2,3}$ and $J_{3,4}$ coupling constants for **4** and 4H^+ would indicate ${}^4\text{C}_1 : {}^1\text{C}_4$ population ratios $\sim 38 : 62$ (**4**) and $27 : 73$ (4H^+).

When CD₃OD was substituted for D₂O, the coupling constants, $J_{1,2} = 1.9$, $J_{2,3} = 4.7$ and $J_{3,4} = 4.4$ Hz, in **4** were all reduced, suggesting an increased proportion of ${}^1\text{C}_4$ in the ${}^4\text{C}_1 \rightleftharpoons {}^1\text{C}_4$ equilibrium but an additional reduction on protonation, $J_{1,2} = 1.7$, $J_{2,3} = 4.1$ and $J_{3,4} = 3.9$ Hz, indicated a further shift, $\sim 10\%$, in the equilibrium in $4\cdot\text{H}^+$ towards ${}^1\text{C}_4$. Solvent dependent variations in the ratio ${}^4\text{C}_1 : {}^1\text{C}_4$, were also revealed through measurements of the corresponding coupling constants in DMSO-d₆, CDCl₃ : CD₃OD (9 : 1), Table S1†; in each case protonation shifted the equilibria towards ${}^1\text{C}_4$.

In summary, while the β anomer retains its ${}^4\text{C}_1$ conformation on protonation and therefore, the equatorial orientation of the charged aglycone, the α anomer displays a solvent dependent dynamic equilibrium between the ${}^4\text{C}_1$ and ${}^1\text{C}_4$ conformations, as expected,¹⁹ which is consistently displaced towards ${}^1\text{C}_4$ on protonation, to create an ion with an equatorially-oriented cationic substituent. What happens when the solvent is removed?

Conformations in the gas phase: vibrational spectroscopy

Protonated Xyl-imidazolium ions $3\cdot\text{H}^+$ and $4\cdot\text{H}^+$ were created in the gas phase through proton transfer following UV laser photo-ionization of their complexes with phenol, formed in a molecular beam (Supplementary Information†, Scheme S2).²⁰ Since the

ions were created through a strongly exothermic proton transfer reaction they were endowed with considerable internal energy²⁰ and assuming a statistical distribution, their temperature could be estimated to be ~ 300 – 350 K—comparable to their temperature in solution. They were detected mass spectrometrically and probed through IR laser multi-photon dissociation spectroscopy (IRMPD) by monitoring the depletion in the parent ion signal when the laser frequency was scanned across their OH, NH and CH vibrational absorption bands. Their IRMPD action spectra are shown in Fig. 4a,d, where they can be compared with computed vibrational spectra associated with alternative low energy structures§ obtained using density functional theory implemented in the Gaussian 03 suite of programs (see Fig. 4b,c,e,f,g).²¹

There were clear differences between the vibrational spectra of the two anomers (Fig. 4a,d) and each one was in excellent accord with the theoretically predicted spectrum associated with their most stable structures. The two spectra, observed as single conformers, confirmed the expected protonation at the distal, N-3' site (compare Fig. 4b,e with Fig. 4c,f) and established a change of the pyranose ring conformation from ${}^4\text{C}_1$ in the protonated β anomer $3\cdot\text{H}^+$ (Fig. 4b) to ${}^1\text{C}_4$ in the corresponding α anomer $4\cdot\text{H}^+$ (Fig. 4e). The inversion, which switches the orientation of the three OH groups from equatorial to axial, promotes hydrogen bonding between the *syn*-diaxial OH₂ and OH₄ groups and this is directly reflected in the different OH vibrational signatures associated with the ${}^4\text{C}_1$ (Fig. 4b and 4g) and the inverted ${}^1\text{C}_4$ conformations (Fig. 4e). In the latter case, the displaced (and broadened) OH₂ band appeared as a shoulder on the high wave number side of the NH⁺ band, shifted by ~ 120 cm⁻¹ toward lower wavenumbers; this reduced the OH triplet, centred ~ 3650 cm⁻¹ in the protonated β anomer $3\cdot\text{H}^+$, Fig. 4a,b, to a doublet in the corresponding α anomer $4\cdot\text{H}^+$, Fig. 4d,e. The absence of any detectable contribution from an underlying triplet component in Fig. 4d, also excluded any significant population of ions in the alternative, ${}^4\text{C}_1$ conformation, see Fig. 4g, consistent with the large calculated difference in their relative energies and free energies (see below).

A similar OH triplet was also observed in the IRMPD spectrum of the β anomer of the pyridinium, Xyl-Pyr⁺ cation, **1**⁺, recorded following the UV photo-oxidation of its neutral parent **1**·H, and shown in Fig. 5 together with its calculated structure

Table 1 Selected ¹H NMR *J* values and conformational equilibria of neutral and protonated α and β D-xylopyranosyl imidazole, **3**, **4**, $3\cdot\text{H}^+$ and $4\cdot\text{H}^+$ in aqueous (D₂O) solution

Compound	Protons	${}^{2/3}J_{\text{H,H}}/\text{Hz}$	${}^4J_{\text{H,H}}/\text{Hz}$	Conformer
3	H1	$J_{1,2} = 9.2$	—	${}^4\text{C}_1$
	H4	$J_{4,5\text{ax}} = 10.6, J_{4,3} = 9.2$	—	
	H5eq	$J_{5\text{eq},5\text{ax}} = 11.4, J_{5\text{eq},4} = 5.5$	—	
$3\cdot\text{H}^+$	H1	$J_{1,2} = 9.2$	—	${}^4\text{C}_1$
	H4	$J_{4,5\text{ax}} = 10.6, J_{4,3} = 9.2$	—	
	H5eq	$J_{5\text{eq},5\text{ax}} = 11.4, J_{5\text{eq},4} = 5.5$	—	
4	H1	$J_{1,2} = 3.0$	—	${}^4\text{C}_1 \rightleftharpoons {}^1\text{C}_4$
	H2	$J_{2,3} = 5.6$	$J_{2,4} = 0.7$	
	H3	$J_{3,4} = 5.1$	$J_{3,5\text{eq}} = 1.1$	
	H4	$J_{4,5\text{eq}} = 5.0, J_{4,5\text{ax}} = 2.9$	—	
	H5eq	$J_{5\text{eq},5\text{ax}} = 11.4, J_{5\text{eq},4} = 5.5$	—	
$4\cdot\text{H}^+$	H1	$J_{1,2} = 2.3$	—	${}^4\text{C}_1 \rightleftharpoons {}^1\text{C}_4$
	H3	$J_{2,3} = 4.9$	$J_{2,4} = 0.9$	
	H2	$J_{3,4} = 4.4$	$J_{3,5\text{eq}} = 1.1$	
	H4	$J_{4,5\text{eq}} = 5.0, J_{4,5\text{ax}} = 2.9$	—	
	H5eq	$J_{4,5\text{eq}} = 3.6, J_{4,5\text{ax}} = 2.5$	—	

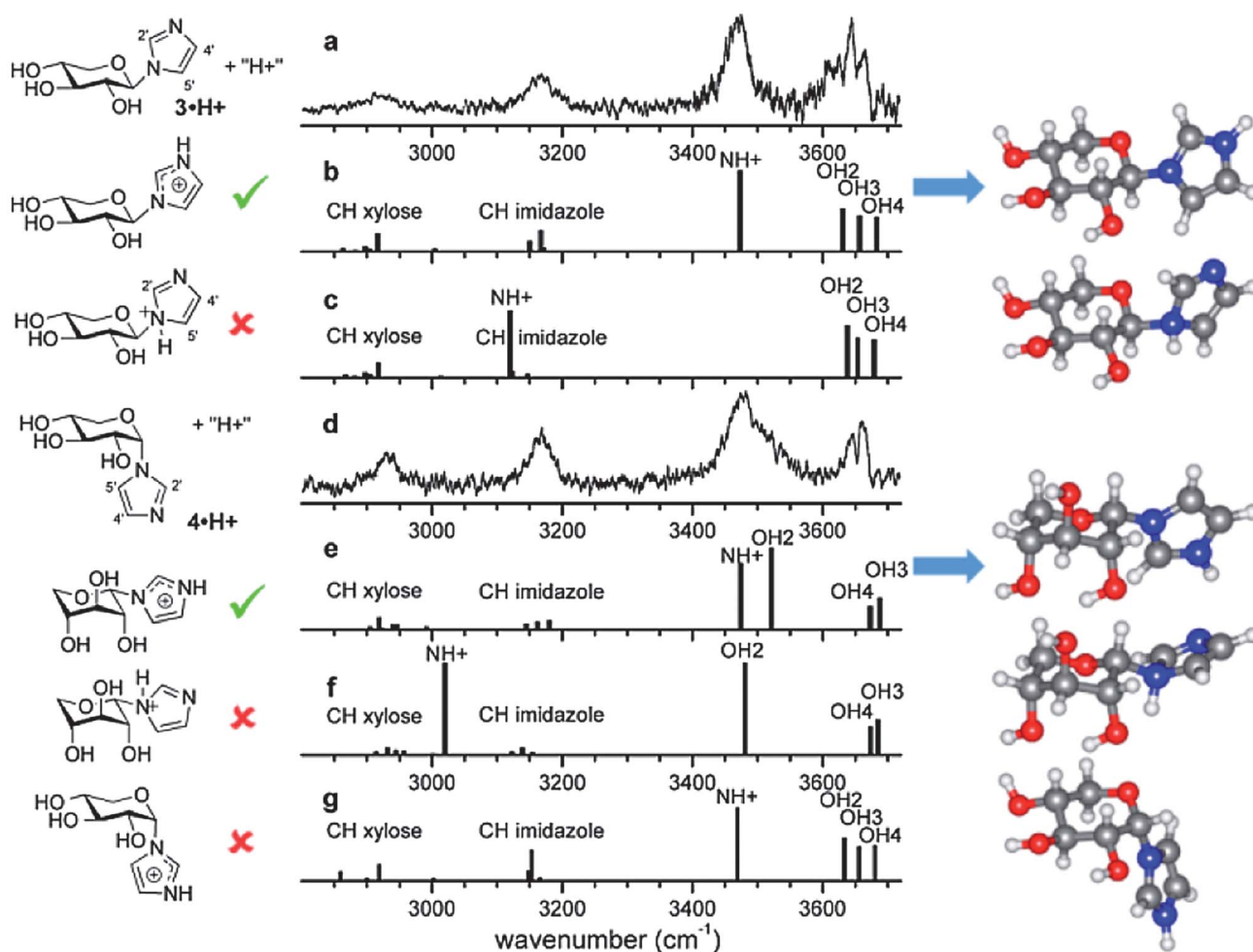


Fig. 4 IR multiphoton dissociation (IRMPD) spectra of the protonated imidazolium ions, Xyl-ImH⁺ **3·H⁺** (a) and **4·H⁺** (d) and the computed vibrational spectra of their minimum energy conformers, protonated on N3' (b,e) or N1' (c,f) and the lowest energy ⁴C₁ conformer of **4·H⁺** (g). Calculations were conducted at the B3LYP/6-311++G(d,p) level and harmonic vibrational frequencies were scaled by 0.9588. The best-fit spectra are indicated with a green 'tick'.

and associated spectrum. (As explained earlier, it was not possible, unfortunately, to record the corresponding spectrum of the α Xyl-Pyr⁺ cation, **2⁺**.)

Density functional theory and *ab initio* calculations

Fig. 6 and 7 present the low energy structures of the neutral and protonated α and β anomers, **3**, **3·H⁺** and **4**, **4·H⁺**, together with their corresponding relative energies at 0 K (including zero point corrections) and free energies at 298 K (including thermal and zero point corrections).

The optimised lowest energy structures of the neutral and protonated β anomer **3** and **3·H⁺**, shown in Fig. 6, both display ⁴C₁ conformations (as do all their computed structures, calculated at relative energies up to at least ~ 20 kJ mol⁻¹). In the protonated ion, the imidazolium substituent is rotated about the C1–N1' bond and the relative orientation of the OH groups in the ion is reversed, from counterclockwise to clockwise. This could be encouraged by charge repulsion between the neighbouring H5' and H2 atoms: a natural bond orbital analysis predicts an increase in their positive charges, $\sim 0.07e$ and $\sim 0.02e$ respectively, following protonation. A

similar reversal in the OH orientation can be seen in the minimum energy structure of the β pyridinium ion, **1⁺**, see Fig. 5. The changed orientation in **3·H⁺**, brings the CH2' and CH5' groups on the imidazolium ion into proximity with O5 and O2, respectively, $r(\text{CH2}'\cdots\text{O5}) \sim 2.36$ Å, $r(\text{CH5}'\cdots\text{O2}) \sim 2.38$ Å and together with the enhanced positive charges on the H2' and H5' atoms, this might promote a weak hydrogen bonded interaction. The delocalisation of the positive charge away from the protonated N3' atom is also signalled by the reduction of the bond length $r(\text{C2}'\cdots\text{N1}')$ from 1.373 Å to 1.335 Å, and by the lowering of the natural charge on N1', from $-0.45e$ to $-0.38e$.

The conformational landscapes of the neutral and protonated α anomer **4** and **4·H⁺**, Fig. 7, are quite different. Their minimum energy structures both present an inverted ¹C₄ conformation; low energy ⁴C₁ conformers are predicted for the neutral at slightly higher energies, ≥ 3 kJ mol⁻¹ but in the ion they lie at much higher energies, ≥ 9 kJ mol⁻¹, which would account for the undetectable population of this conformer in the experimental IRMPD spectrum, as we have previously noted, even at 300–350 K. Protonation again rotates the imidazolium substituent about the C1–N1' bond (but this time to bring CH2' into

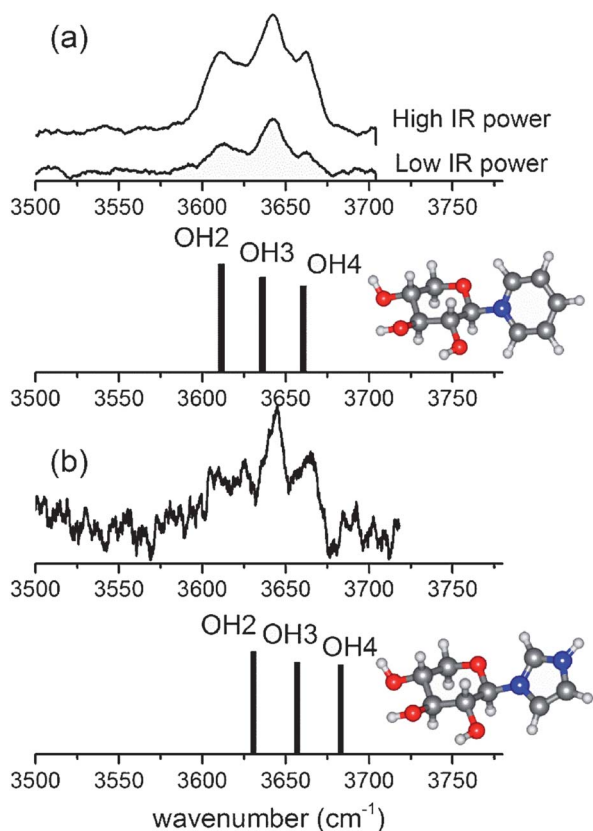


Fig. 5 Comparison of the IRMPD spectra of (a) β xylopyranosyl pyridinium, Xyl-Pyr+ 1^+ (recorded at high and low IR laser powers) and (b) β xylopyranosyl imidazolium $3 \cdot H^+$, together with the computed vibrational spectra and structures of their corresponding lowest energy conformers. (Calculations for 1^+ conducted at the B3LYP/6-31+G(d) level and harmonic vibrational frequencies scaled by 0.9733.)

proximity with O2) and the orientation of the OH groups, now axial and reversed, reduces the *syn* diaxial hydrogen bond distance from 2.05 Å, $r(OH4 \cdots O2)$ in **4**, to 1.91 Å, $r(OH2 \cdots O4)$

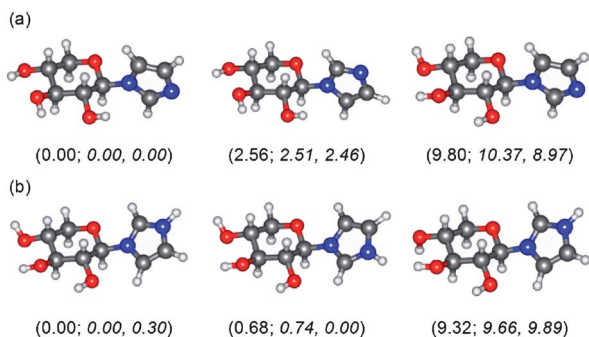


Fig. 6 Lowest energy structures and relative energies of (a) neutral and (b) protonated β D-xylopyranosyl imidazole, **3** and $3 \cdot H^+$. The bracketed numbers indicate the energies calculated using MP2/6-311++G(d,p)//B3LYP/6-311++G(d,p) (at 0 K) and, in italics, the energies (at 0 K) and free energies (at 298 K) calculated using M06-2X/6-31+G(d,p). The structures calculated using the M06-2X functional, although including the influence of dispersion interactions, were virtually identical to those calculated using B3LYP shown here, which do not. Further details are provided as Supplementary Information†, Tables S3–8.

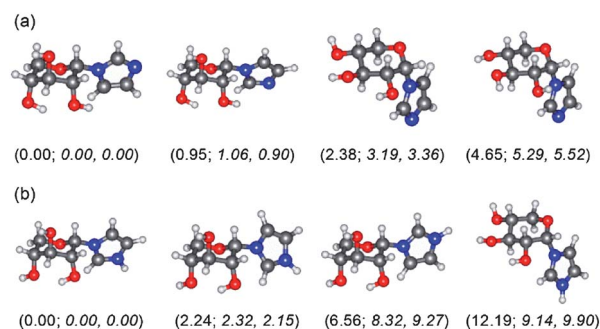


Fig. 7 Lowest energy structures, relative energies at 0 K and free energies at 298 K (kJ mol^{-1}) of (a) neutral **4** and (b) protonated α D-xylopyranosyl imidazole $4 \cdot H^+$, calculated using MP2/6-311++G(d,p)//B3LYP/6-311++G(d,p) (0 K) and (in italics) M06-2X/6-31+G(d,p) (at 0 K and 298 K).

in $4H^+$, to provide additional stabilisation. There are also suggestions of steric interactions in the lowest energy 4C_1 conformers of the neutral and protonated ions **4**, $4 \cdot H^+$, between O2 and the neighbouring N1' and C2' atoms on the imidazole substituent. In the neutral molecule the N1'...O2 and C2'...O2 separations are both ~ 2.95 Å, but in the corresponding (higher energy) conformer of the ion, they are somewhat closer, respectively ~ 2.88 Å and ~ 2.78 Å, all within the van der Waals radii.

Concluding remarks

In the neutral α anomer **4**, the balance between the favoured 1C_4 (aglycone equatorial) conformation and the 'normal' 4C_1 (aglycone axial) conformation is a fine one. As Vaino and Szarek remarked,⁵ "the xylo configuration can be considered to be spring-loaded", making xylose an ideal choice for study. The preference for the inverted structure (which lies only 2–3 kJ mol^{-1} below the aglycone axial structure) is aided by the reversed orientation of the diaxially oriented OH2 and OH4 groups and the consequent enhanced hydrogen bonding between them, $r(OH4 \cdots O2) \sim 2.05$ Å, cf. $r(OH2 \cdots O4) \sim 2.37$ Å; the relief of the steric interaction between O2 and the neighbouring atoms, N1' and C2' on the imidazole group; and also, perhaps, a favourable antiparallel dipolar interaction, see Fig. 8.⁵

In the protonated ion $4 \cdot H^+$, where the normal 4C_1 (axial) anomeric conformation is not observed (it lies at least 9 kJ mol^{-1} above the inverted 1C_4 lowest energy conformation) these interactions are markedly enhanced. There is a much more pronounced increase in the diaxial hydrogen bonded interaction in the 1C_4 conformer, where $r(OH2 \cdots O4) \sim 1.91$ Å and a rather closer steric interaction in the 4C_1 conformer, where the O2...N1'

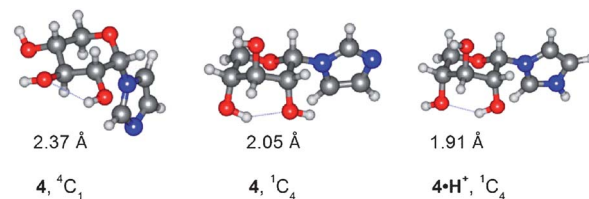


Fig. 8 Hydrogen bonded interactions in neutral and protonated α D-xylopyranosyl imidazole.

and O2...C2' separations decrease to 2.88 Å and 2.78 Å, respectively, *cf.* 2.95 Å in the neutral anomer **4**. Again quoting Vaino and Szarek,⁵ “the proton acts as the straw that breaks the camel’s back”; the conformational changes promoted by protonation act to overwhelm fully, the normal anomeric effect.

Although the relative populations of the normal and inverted conformations of the pyranose ring in solution vary with the nature of the solvent, the overall behaviour of the neutral and protonated anomers of Xyl imidazole broadly parallels expectations based on the DFT calculations for the isolated anomers and the experimental results obtained for their ions in the gas phase. The primary factors determining the variations in conformational choice in the neutral and protonated ion do not reflect environmental effects but rather, the relative strengths of their internal, non-covalent interactions.

Acknowledgements

We thank Dr P. Çarçal for help with experimental measurements; Dr E. C. Stanca-Kaposta for early computational work; EPSRC for funding (GR/T26542, EP/E000614/1); the Leverhulme Trust for an Emeritus Fellowship (JPS); the Royal Society for a USA/Canada Research Fellowship and Linacre College for a Junior Research Fellowship (TDV); and STFC for provision of equipment from the Laser Loan Pool. BGD is a Royal Society Wolfson Research Merit Award recipient and is supported by an EPSRC LSI Platform grant.

Notes and references

‡ The ¹H spectrum of **4** was not amenable to direct analysis owing to complexity from second-order coupling (resonance overlap of H4 with H5eq) requiring complete spin-system simulation (Supplementary Information†, Figure S5).

§ The relative intensities of IRMPD spectra depend on the probability of molecular dissociation following the initial excitation of each selected vibrational mode; the bands are also broadened by the internal excitation of the ions. The computed IR absorption bands, displayed as ‘stick’ spectra, take no account of these factors but their frequencies provide a reliably accurate basis for comparisons with experimental data.¹⁸

- 1 R. U. Lemieux and A. R. Morgan, *Can. J. Chem.*, 1965, **43**, 2205.
- 2 R. U. Lemieux, *Pure Appl. Chem.*, 1971, **27**, 527.
- 3 H. Paulsen, Z. Györgydeák and M. Friedmann, *Chem. Ber.*, 1974, **107**, 1590.
- 4 A. R. Vaino, S. S. C. Chan, W. A. Szarek and G. R. J. Thatcher, *J. Org. Chem.*, 1996, **61**, 4514.
- 5 A. R. Vaino and W. A. Szarek, *J. Org. Chem.*, 2001, **66**, 1097.
- 6 I. Tvaroška and J. P. Carver, *J. Phys. Chem.*, 1996, **100**, 11305.
- 7 C. J. Cramer, *J. Org. Chem.*, 1992, **57**, 7034.
- 8 C. L. Perrin, *Tetrahedron*, 1995, **51**, 11901.
- 9 C. L. Perrin, *Pure Appl. Chem.*, 1995, **67**, 719.
- 10 C. L. Perrin and K. B. Armstrong, *J. Am. Chem. Soc.*, 1993, **115**, 6825.
- 11 C. L. Perrin, M. A. Fabian, J. Brunckova and B. K. Ohta, *J. Am. Chem. Soc.*, 1999, **121**, 6911.
- 12 P. G. Jones, A. J. Kirby, I. V. Komarov and P. D. Wothers, *Chem. Commun.*, 1998, 1695.
- 13 C. S. Rye and S. G. Withers, *J. Org. Chem.*, 2002, **67**, 4505.
- 14 K. D. Randell, B. D. Johnston, D. F. Green and B. M. Pinto, *J. Org. Chem.*, 2000, **65**, 220.
- 15 H. Grundberg, J. Eriksson-Bajtner, K.-E. Bergquist, A. Sundin and U. Ellervik, *J. Org. Chem.*, 2006, **71**, 5892.
- 16 E. Juaristi and G. Cuevas, *J. Am. Chem. Soc.*, 1993, **115**, 1313.
- 17 M. Mikolajczyk and P. P. Graczyk, *J. Org. Chem.*, 1995, **60**, 5190.
- 18 S. Rudić, H.-B. Xie, R. B. Gerber and J. P. Simons, *Mol. Phys.*, 2012, DOI: 10.1080/00268976.2012.660206.
- 19 C. L. Perrin and J. Kuperman, *J. Am. Chem. Soc.*, 2003, **125**, 8846.
- 20 (a) N. A. Macleod and J. P. Simons, *Mol. Phys.*, 2007, **105**, 689; (b) T. D. Vaden, T. S. J. A. de Boer, N. A. MacLeod, E. M. Marzluff, J. P. Simons and L. C. Snoek, *Phys. Chem. Chem. Phys.*, 2007, **9**, 2549; (c) T. D. Vaden, T. S. J. A. de Boer, J. P. Simons, L. C. Snoek, G. Suhai and B. Paizs, *J. Phys. Chem. A*, 2008, **112**, 4608.
- 21 (a) M. J. Frisch *et al.*, *Gaussian 03, Revision B.04*, Gaussian, Inc., Pittsburgh, PA, 2003; (b) M. J. Frisch *et al.*, *Gaussian 09, Revision A.02*, Gaussian Inc., Wallingford CT, 2009.